

Supporting Information

Interconversion Rates between Conformational States as Rationale for the Membrane Permeability of Cyclosporines

Jagna Witek,^[a] Max Mühlbauer,^[a] Bettina G. Keller,^[b] Markus Blatter,^[c] Axel Meissner,^[c] Trixie Wagner,^[c] and Sereina Riniker*^[a]

cphc_201700995_sm_miscellaneous_information.pdf

SUPPLEMENTARY MATERIAL

Jagna Witek,[†] Max Mühlbauer,[†] Bettina G. Keller,[‡] Markus Blatter,[¶] Axel
Meissner,[¶] Trixie Wagner,[¶] and Sereina Riniker^{*,†}

[†]*Laboratory of Physical Chemistry, ETH Zürich, Vladimir-Prelog-Weg 2, 8093 Zürich,
Switzerland*

[‡]*Department of Biology, Chemistry, Pharmacy, Freie Universität Berlin, Takustrasse 3,
14195 Berlin, Germany*

[¶]*Novartis Institutes for BioMedical Research, Novartis Pharma AG, Novartis Campus,
4056 Basel, Switzerland*

E-mail: sriniker@ethz.ch

Experimental Methods

Sample Preparation

3.5 mg of lyophilized cyclosporine E (CsE) were dissolved in either 35 μ l d6-DMSO, 40 μ l de-acidified CDCl₃, or 40 μ l CCl₄ (5% C₆D₆), vortexed for 20 s and transferred into 1.7 mm SampleJet NMR sample tubes. Samples were spun down into the tube using a Hettich manual centrifuge. Tubes were then closed by pressing a POM ball into the funnel of the tube cap. Tubes were then inserted into 1.7 mm shuttles and placed on the automatic sample changer.

Data Acquisition and Processing

¹H detected 1D and 2D NMR spectra were obtained using a Bruker 600 MHz AVANCE III spectrometer equipped with a 1.7 mm TCI cryo probe and a *z*-gradient system. 1D proton spectra were recorded with a standard one-pulse sequence (30 ° flip angle) with a relaxation delay of 1 s and an acquisition time of 2.73 s. 16 scans of 65536 points covering 12019.23 Hz were recorded. For determination of amide temperature coefficients data was recorded in a range of 290–320 K for DMSO and 275–300K for chloroform and CCl₄, respectively. Data was zero-filled to 65536 complex points and an exponential window function was applied with a line-broadening factor of 0.3 Hz prior to Fourier transformation.

All 2D experiments for NMR assignment were recorded at a temperature of 300 K with a relaxation delay of 1.5 s. For gradient COSY spectra^{1,2} a data matrix of 512 x 2048 points covering 6602.1 x 6602.1 Hz was recorded with one scan for each increment. Data was linear predicted to 1024 x 2048 points using 32 coefficients and zero filled to 2048 x 2048 points. A sine square bell shaped window function was applied in F2 and a cosine square bell shaped window function in F1, respectively, prior to magnitude mode type 2D Fourier transformation. For edited coherence order selective gradient HSQC spectra^{3,4} using adiabatic inversion pulses on the carbon channel, a data matrix of 256 x 2048 points covering

24901 x 8417.5 Hz was recorded using two scans for each increment. Data was linear predicted to 512 x 2048 points using 32 coefficients and zero filled to 1024 x 2048 points prior to echo-anti echo type 2D Fourier transformation. A sine square bell shaped window function shifted by $\pi/2$ in both dimensions was applied. For HMBC spectra⁵ a data matrix of 320 x 4096 points covering 33805 x 8417.5 Hz with eight scans for each increment was recorded using a double low pass J-filter and F1 absorption mode.⁶ Data was linear predicted to 640 x 4096 points using 32 coefficients and zero-filled to 1024 x 2048 complex points prior to echo-anti echo type 2D Fourier transformation. A cosine square shaped window function was applied in F1 and a sine shaped window function shifted by $\pi/4$ was applied in F2. Data was converted to magnitude mode in F2 prior to analysis. ROESY spectra^{7,8} with an effective field of $\gamma B_1 = 8333$ Hz and an spin lock time of 200 ms were recorded for a data matrix of 512 x 2048 points covering 8417.5 x 8417.5 Hz. Eight scans were recorded for each increment. Data was linear predicted to 1024 x 2048 points using 32 coefficients prior to States-TPPI type 2D Fourier transformation and a sine square bell shaped window function shifted by $\pi/2$ in both dimensions was applied. For MLEV-17 based TOCSY spectra⁹ a data matrix of 512 x 2048 points covering 8417.5 x 8417.5 Hz two scans were recorded for each increment. Data was linear predicted to 1024 x 2048 points using 32 coefficients and zero filled to 1024 x 2048 complex points prior to TPPI type 2D Fourier transformation. A cosine square bell shaped window function was applied in both dimensions. For determination of $^n_{HC}$ couplings constants J-HMBC spectra¹⁰ were acquired. A folded data matrix of 1024 x 4096 points covering 21128.5 x 6602.1 Hz was recorded using 16 scans for each increment. A coupling evolution delay of 436.8 ms with a scaling factor of 18 was used. Data was linear predicted to 2048 x 4096 points using 32 coefficients and zero-filled to 2048 x 4096 complex points prior to echo-anti echo type 2D Fourier transformation. A cosine square shaped window function was applied in F1 and a sine shaped window function shifted by $\pi/4$ was applied in F2. Data was converted to magnitude mode in F2 prior to analysis. For determination of coupling constants relevant 1D traces along F1 were extracted using Topspin 3.2 (Bruker Biospin).

All spectra were referenced according to the internal solvent signal (1H: d6-DMSO = 2.50 ppm and 13C: d6-DMSO = 39.52 ppm; 1H: CDCl₃ = 7.26 ppm and 13C: CDCl₃ = 77.16 ppm; 1H: C6D6 = 7.16 ppm and 13C: C6D6 = 128.06 ppm).¹¹

Resonance Assignment

1D and 2D spectra were imported into the NMR workbook of ACD Spectrus 2014 for resonance assignment. 1D, HSQC and TOCSY were analyzed to assign protons and carbons of individual amino acid spin systems. Sequential connectivity assignments were achieved using 2D-NOESY experiments.

Structure Calculation

Initial peak picking and nOe assignments were performed using the ATNOSCANDID package.^{12,13} Peak lists of the first cycle were used as an input for the program CYANA 3.97.¹⁴ The peaklist was analyzed in SPARKY and inter-strand NOEs were assigned manually. In presence of dihedral restraints based on homo and hetero ³J scalar couplings using the Karplus equation, the "noeassign" protocol of CYANA was used to assign unassigned peaks and calibrate the nOe signals with an average NOE distance of 0.42 nm. The resulting upper distance lists were cleaned by applying a cutoff for the support factor of 0.3 and by reviewing the peak lists and inspection of the NOESY spectra.

The AMBER 14 package¹⁵ was used for structure refinement in implicit solvent (GB Neck variant of the generalized Born model¹⁶) using dielectric constants of 2 or 46.7 reflecting the non-polar solvent CCl₄ and the polar solvent DMSO. Using antechamber,¹⁷ parameters were written based on AM1-BCC partial charges in combination with the GAFF¹⁸ force field. Harmonic square-well penalty functions with force constants of 10 kcal mol⁻¹ Å⁻² for all distance constraints were applied. An exception was made for the distance restraints between the *N*-methyl groups (*i*) and α-protons (*i*-1) of *trans* peptide bonds and between the two α-protons of the *cis* peptide bond of residue 9/10. In these cases, the restraining

force constant was set to 50 kcal mol⁻¹ Å⁻² to ensure the correct conformation.

First, a short minimization with long-range electrostatics treatment by the particle mesh Ewald method¹⁹ using steepest descents energy minimization followed up with conjugate gradient minimization was performed. The minimized structures were then refined using a simulated annealing protocol of 30'000 steps. For all refinements, a time step of 1 fs in combination with constrained bond lengths by applying SHAKE²⁰ and a non-bonded cutoff of 1.5 nm were used. The scaling factors for the 1,4-electrostatic and 1,4-Lennard-Jones interactions were set to default values (scee = 1.2, scnb = 2.0). For each solvent, all ten conformers of CsE were refined using AMBER for the final ensembles.

Computational Methods

All simulations were performed using the GROMOS software package²¹ and the GROMOS 54A7 force field.²² As “closed” starting conformation of CsE in an apolar environment, the available small-molecule crystal structure (ID: SUQNUN,²³ source: Cambridge Structure Database) was taken. Due to the lack of an experimentally determined structure of CsE in polar solvents, coordinates of an “open” starting structure were created by replacing the Val-11 N-methyl group with a hydrogen atom in the crystal structure of CsA co-crystallized with cyclophilin in water (ID: 2Z6W,²⁴ source: Protein Data Bank (PDB)). Both structures were used for MD simulations of CsE in water, DMSO, chloroform and tetrachloromethane (CCl₄). To enhance sampling, Hamiltonian replica exchange (HRE)²⁵ and temperature replica exchange (TRE)²⁶ simulations were performed in water, DMSO, chloroform and CCl₄. The HRE simulations involved six replicas with the force constant on all backbone torsion angles being scaled by 1.0, 0.8, 0.6, 0.4, 0.2, and 0.0, respectively. The TRE simulations involved temperature scaling from 300 K to 400 K using 21 replicas. The HRE and TRE simulations were 50 ns long, preceded by 100 ps of equilibration. In water and DMSO, the ?closed? conformation was used as starting structure, whereas the ?open? conformation was

used in chloroform and CCl₄.

All production simulations were of 100 ns length, preceded by 100 ps of equilibration. In the next step, the 100 most diverse conformations from each simulation (MD and HRE), were selected based on the backbone torsion RMSD, using the **LazyPicker** program from the RDKit suite.²⁷ Subsequently, the 100 most diverse conformations from each solvent were pooled, and the **LazyPicker** was used again to select from this pool the final 100 most diverse conformations. Starting from each of the seed conformations obtained in the previous step, a MD simulation of 100 ns length was performed at 300 K in each solvent, resulting in total 10 μ s simulation data for each solvent. The simulation trajectories were used further to construct MSMs of CsE. The features of the MSM theory have been discussed in detail elsewhere.^{28–30} In short, the trajectories were discretized by assigning each snapshot to a microstate. The microstates were obtained by clustering the 10 μ s simulation in each solvent separately based on the backbone torsion RMSD (cutoff = 20°), and then clustering again all centroids of clusters with more than 10 members of all solvents together (using the same cutoff). This resulted in 521 clusters centroids, which were used to define the microstates. As this conformational clustering for discretization was performed using the simulation data of all solvents, it is possible to directly compare the microstates in the different environments. The resulting MSMs provide information about implied timescales (ITS) of interconversion processes occurring in each solvent. The Perron Cluster-Cluster Analysis plus (PCCA+)^{28,31,32} method was employed to identify metastable sets, representing long-lived conformations of a molecule. PCCA+ was used in a sequential manner, i.e. increasing the number of metastable sets iteratively, to obtain the hierarchy of the energy barriers. The ITS of MSM obtained from 10 μ s simulations in water and DMSO did not reach convergence. To resolve this issue, a resampling procedure was employed, resulting in total 20 μ s of simulation data in water and DMSO. For this, additional seed conformations were selected from the HRE simulations, and subsequently a 100 ns simulation was performed for each. The conformational space sampled during the total 10-20 μ s simulation is represented

by the Ramachandran plots of the backbone torsion angles, shown in Figs. S3 - ??.

Additional Tables and Figures

Table S1: NOE upper distance bounds of CsE in CCl₄. The atom labels are shown in Fig. S1.

Index	Residue 1	Residue 2	Upper bound [nm]
1	1 HA	6 HA	0.424
2	1 HA	7 HN	0.421
3	2 HN	5 HN	0.438
4	11 HN	8 HN	0.533
5	2 HN	5 HB	0.552
6	6 HD	1 HA	0.592
7	2 HB	5 HB	0.509
8	8 HN	6 HB	0.462
9	1 HG1	3 HCN	0.505
10	8 HA	6 HD	0.352
11	8 HN	7 HN	0.386
12	7 HN	6 HA	0.361
13	10 HA	10 HCN	0.404
14	1 HCN	2 HA	0.472
15	4 HCN	5 HN	0.310
16	3 HCN	3 HA	0.384
17	1 HA	2 HG	0.473
18	9 HG	8 HA	0.361
19	9 HG	9 HCN	0.48
20	5 HN	5 HB	0.404
21	5 HB	6 HCN	0.369
22	8 HN	7 HB	0.467
23	7 HN	6 HB	0.476
24	1 HB	2 HN	0.451
25	10 HG	10 HCN	0.600
26	1 HG	1 HA	0.413
27	1 HG	1 HCN	0.411
28	4 HCN	4 HB	0.385
29	4 HCN	4 HB	0.342
30	9 HB	9 HCN	0.351
31	9 HCN	8 HB	0.383
32	8 HB	8 HN	0.355
33	6 HCN	6 HB	0.383
34	1 HD1	1 HA	0.428
35	1 HCN	11 HB	0.501
36	10 HB	10 HCN	0.378

Continued on next page

Index	Residue 1	Residue 2	Upper bound [nm]
37	10 HCN	9 HG	0.600
38	10 HCN	9 HB	0.581
39	11 HG	11 HN	0.399
40	9 HB	9 HCN	0.378
41	5 HN	5 HG1	0.509
42	5 HN	5 HG2	0.436
43	10 HB	9 HA	0.420
44	10 HB	10 HCN	0.550
45	10 HB	10 HCN	0.407
46	4 HCN	5 HB	0.447
47	11 HG	11 HA	0.370
48	10 HD	11 HN	0.440
49	10 HD	10 HA	0.398
50	1 HG1	1 HD2	0.433
51	1 HG1	1 HD1	0.481
52	1 HB	1 HD1	0.386
53	1 HH	1 HE	0.356
54	4 HD	4 HB	0.336
55	10 HD	10 HB	0.228
56	4 HB	5 HG	0.467
57	1 HG1	1 HH	0.476
58	1 HD1	1 HZ	0.437

Table S2: NOE upper distance bounds of CsE in DMSO. The atom labels are shown in Fig. S1.

Index	Residue 1	Residue 2	Upper bound [nm]
1	1 HA	7 HA	0.529
2	1 HA	7 HN	0.398
3	7 HA	2 HN	0.550
4	2 HN	5 HN	0.441
5	2 HN	5 HA	0.575
6	2 HN	6 HA	0.530
7	11 HA	7 HN	0.519
8	11 HN	8 HN	0.572
9	11 HN	7 HN	0.521
10	1 HA	6 HB	0.550
11	1 HA	7 HB	0.423
12	1 HD2	7 HN	0.478
13	7 HN	2 HG	0.499
14	1 HZ	7 HN	0.524
15	1 HZ	6 HCN	0.504
16	2 HN	5 HB	0.560
17	11 HA	7 HB	0.526
18	11 HB	8 HA	0.546
19	11 HB	8 HN	0.470
20	11 HB	7 HN	0.522
21	7 HB	2 HN	0.561
22	1 HD1	7 HN	0.561
23	5 HG	2 HN	0.544
24	11 HG	8 HN	0.549
25	11 HG	7 HN	0.541
26	1 HD2	7 HB	0.533
27	1 HZ	6 HB	0.490
28	1 HZ	6 HD	0.419
29	11 HB	7 HB	0.388
30	1 HB	6 HD	0.523
31	11 HG	7 HB	0.369
32	11 HN	9 HCN	0.508
33	3 HA	5 HN	0.437
34	8 HN	6 HB	0.581
35	5 HG	7 HA	0.592
36	6 HD	8 HN	0.521
37	11 HG	9 HCN	0.489
38	7 HB	5 HB	0.548
39	1 HA	2 HN	0.320
40	1 HA	1 HCN	0.394
41	8 HN	7 HN	0.475
42	7 HN	6 HA	0.304
43	7 HN	6 HCN	0.470
44	2 HN	3 HCN	0.460

Continued on next page

Index	Residue 1	Residue 2	Upper bound [nm]
45	2 HN	3 HA	0.581
46	11 HN	10 HA	0.319
47	11 HN	10 HCN	0.460
48	4 HCN	5 HN	0.412
49	4 HCN	4 HA	0.410
50	1 HCN	2 HN	0.563
51	3 HCN	3 HA	0.307
52	10 HCN	9 HA	0.574
53	1 HA	2 HB	0.550
54	1 HA	2 HG	0.483
55	1 HA	11 HG	0.548
56	9 HA	9 HG	0.389
57	4 HB	5 HN	0.451
58	4 HB	5 HA	0.539
59	1 HG1	2 HN	0.504
60	4 HG	5 HN	0.461
61	4 HG	5 HA	0.499
62	9 HB	9 HCN	0.351
63	9 HB	9 HCN	0.405
64	9 HG	9 HCN	0.418
65	5 HN	5 HB	0.364
66	5 HB	6 HCN	0.405
67	6 HA	6 HG	0.367
68	7 HN	6 HG	0.428
69	7 HN	6 HB	0.516
70	1 HD2	1 HA	0.427
71	1 HD2	2 HN	0.478
72	5 HA	6 HB	0.487
73	5 HA	6 HB	0.526
74	8 HN	7 HB	0.371
75	7 HA	6 HB	0.550
76	7 HA	6 HG	0.550
77	7 HA	6 HD	0.550
78	7 HN	6 HB	0.469
79	7 HN	6 HB	0.468
80	7 HN	6 HD	0.408
81	2 HN	2 HG	0.429
82	2 HN	2 HB	0.357
83	2 HB	3 HCN	0.483
84	11 HB	11 HN	0.387
85	1 HB	2 HN	0.464
86	1 HB	1 HCN	0.421
87	3 HA2	4 HD	0.495
88	10 HB	9 HA	0.477
89	10 HG	10 HCN	0.437
90	4 HA	5 HG	0.510

Continued on next page

Index	Residue 1	Residue 2	Upper bound [nm]
91	1 HG	1 HA	0.414
92	1 HG	1 HCN	0.412
93	4 HCN	4 HG	0.397
94	4 HCN	4 HB	0.378
95	4 HB	5 HN	0.581
96	9 HB	9 HCN	0.350
97	9 HCN	8 HB	0.341
98	1 HD2	1 HA	0.354
99	8 HB	8 HN	0.406
100	8 HB	7 HA	0.455
101	6 HCN	6 HB	0.315
102	7 HB	6 HA	0.429
103	7 HB	7 HN	0.370
104	6 HD	6 HA	0.436
105	1 HD1	1 HA	0.368
106	10 HB	10 HCN	0.334
107	4 HD	4 HCN	0.374
108	9 HD	9 HA	0.412
109	9 HD	9 HCN	0.428
110	5 HG	5 HN	0.389
111	5 HG	5 HA	0.327
112	5 HG	4 HCN	0.433
113	5 HG	6 HCN	0.342
114	6 HD	7 HA	0.469
115	6 HD	7 HN	0.489
116	6 HD	6 HCN	0.492
117	11 HG	11 HA	0.335
118	11 HG	11 HN	0.387
119	11 HG	1 HCN	0.386
120	11 HG	10 HCN	0.532
121	10 HD	10 HCN	0.388
122	9 HB	9 HD	0.412
123	1 HB	1 HD2	0.365
124	1 HB	1 HD1	0.341
125	1 HG	1 HZ	0.370
126	1 HD2	1 HZ	0.324
127	6 HD	6 HB	0.377
128	1 HH	1 HZ	0.287
129	1 HD1	1 HZ	0.370
130	1 HD1	1 HD2	0.336
131	4 HD	4 HG	0.223
132	4 HD	4 HB	0.318
133	9 HD	9 HB	0.310
134	6 HD	6 HG	0.256
135	6 HD	6 HB	0.304

Continued on next page

Index	Residue 1	Residue 2	Upper bound [nm]
136	10 HD	10 HB	0.281

Table S3: $^3J_{\text{HNHA}}$ coupling constants of CsE in CCl_4 and DMSO. The Karplus relationship is of the form $^3J(\phi) = A \cdot \cos^2(\phi) + B \cdot \cos(\phi) + C$ with $A = 7.13$, $B = -1.31$ and $C = 1.56$. The Karplus parameters were estimated following the Bayesian procedure described in Ref. 33. The atom labels are shown in Fig. S1.

Index	Residue 1	Residue 2	$^3J_{\text{HNHA}}$ [Hz] CCl_4	$^3J_{\text{HNHA}}$ [Hz] DMSO
1	2 HN	2 HA	9.8	9.7
2	5 HN	5 HA	8.6	8.6
3	7 HN	7 HA	9.4	8.4
4	8 HN	8 HA	6.4	6.1
5	11 HN	11 HA	9.6	9.5

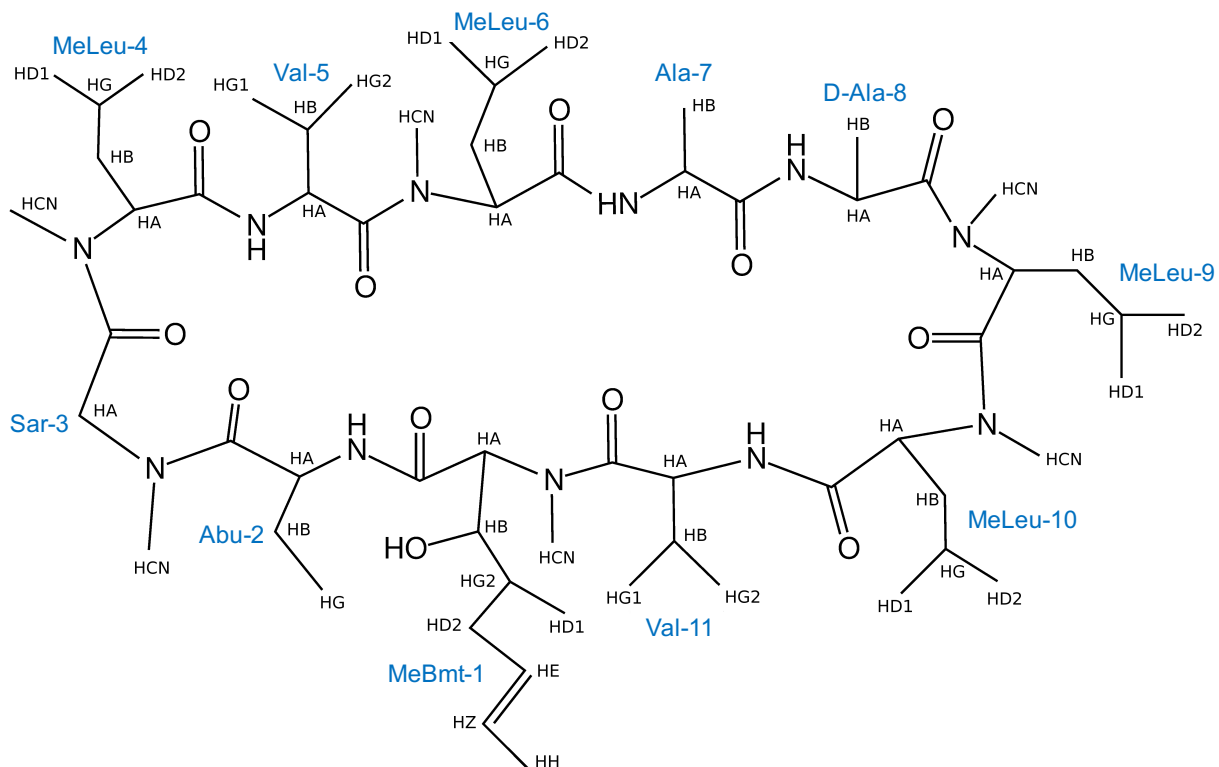


Figure S1: Schematic structure of CsE with atom labels.

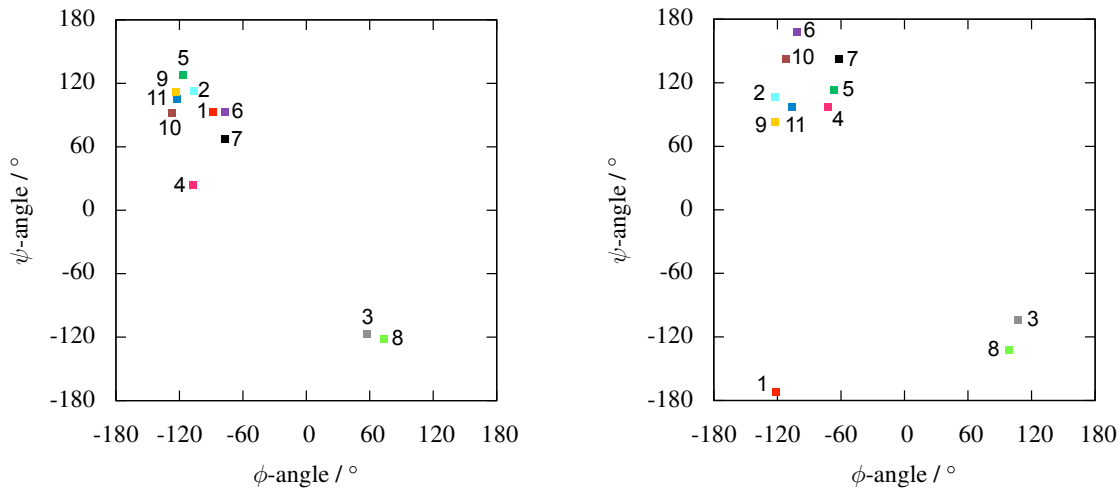


Figure S2: Backbone dihedral angles ϕ and ψ of the 11 residues in the crystal structures of CsA: DEKSAN³⁴ (source: Cambridge Structure Database (CSD)) (left), and 2Z6W²⁴ (source: Protein Data Bank (PDB), co-crystallized with cyclophilin) (right). This replaces Figure 1C in Ref. 35, where the ϕ and ψ angles were not paired correctly. The corrected Ramachandran plots of the 10 μ s simulations of CsA in chloroform and water are shown in Figs. S3 and S4, respectively.

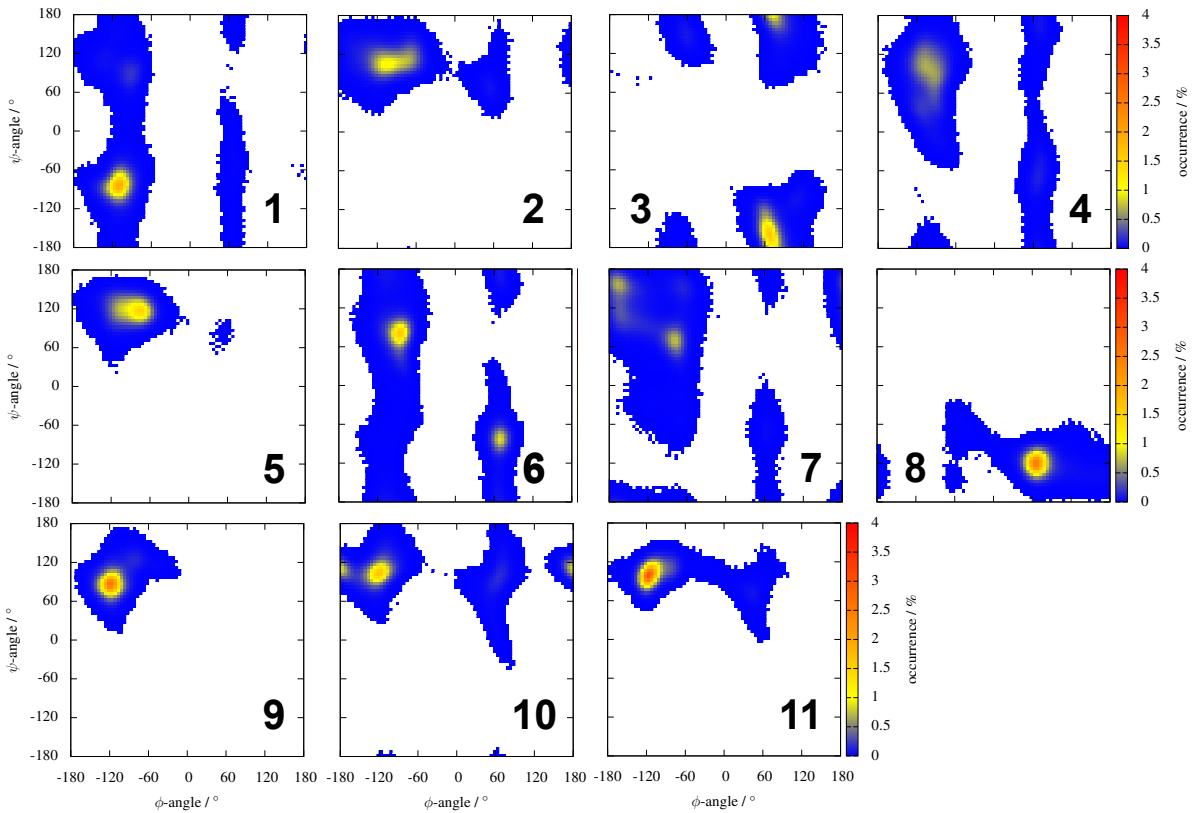


Figure S3: Ramachandran plots for the backbone torsion angles from 10 μ s simulations of CsA in chloroform. This replaces Fig. 5A in Ref. 35, where the ϕ and ψ angles were not paired correctly.

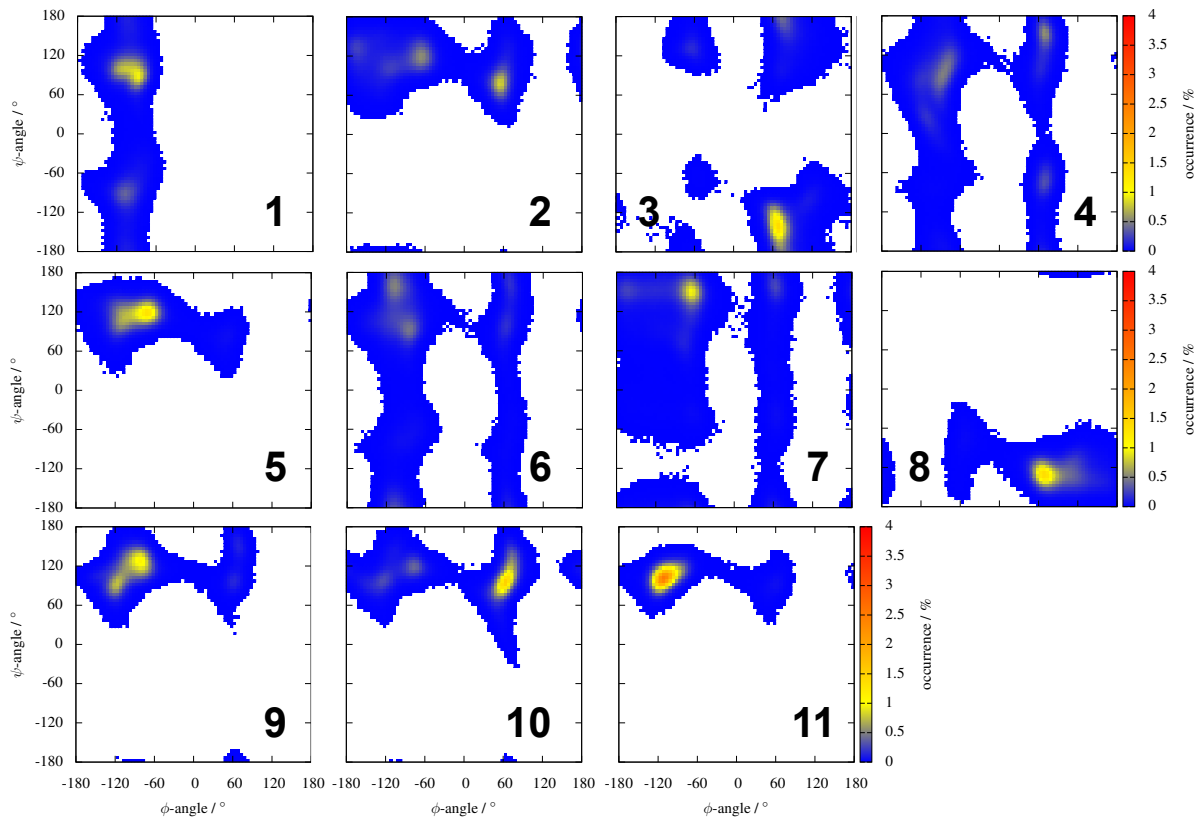


Figure S4: Ramachandran plots for the backbone torsion angles from $10 \mu\text{s}$ simulations of CsA in water. This replaces Fig. 5B in Ref. 35, where the ϕ and ψ angles were not paired correctly.

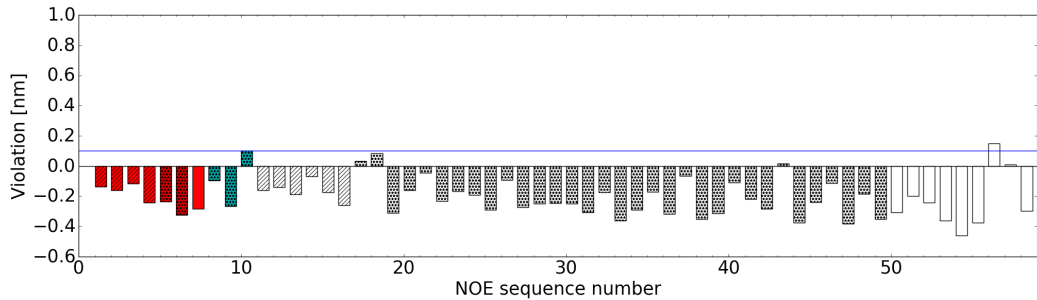


Figure S5: Violations of the experimental NOE upper distance bounds in CCl_4 by the small-molecule crystal structure (CSD: SUQNUN²³). The NOE distances are grouped into “intercycle” (red), “intermediate” (cyan) and “vicinal” (white), and they are labelled on the basis of nature of the hydrogens: backbone–backbone (stripes), backbone–side chains (dot) and side chain–side chain (plain).

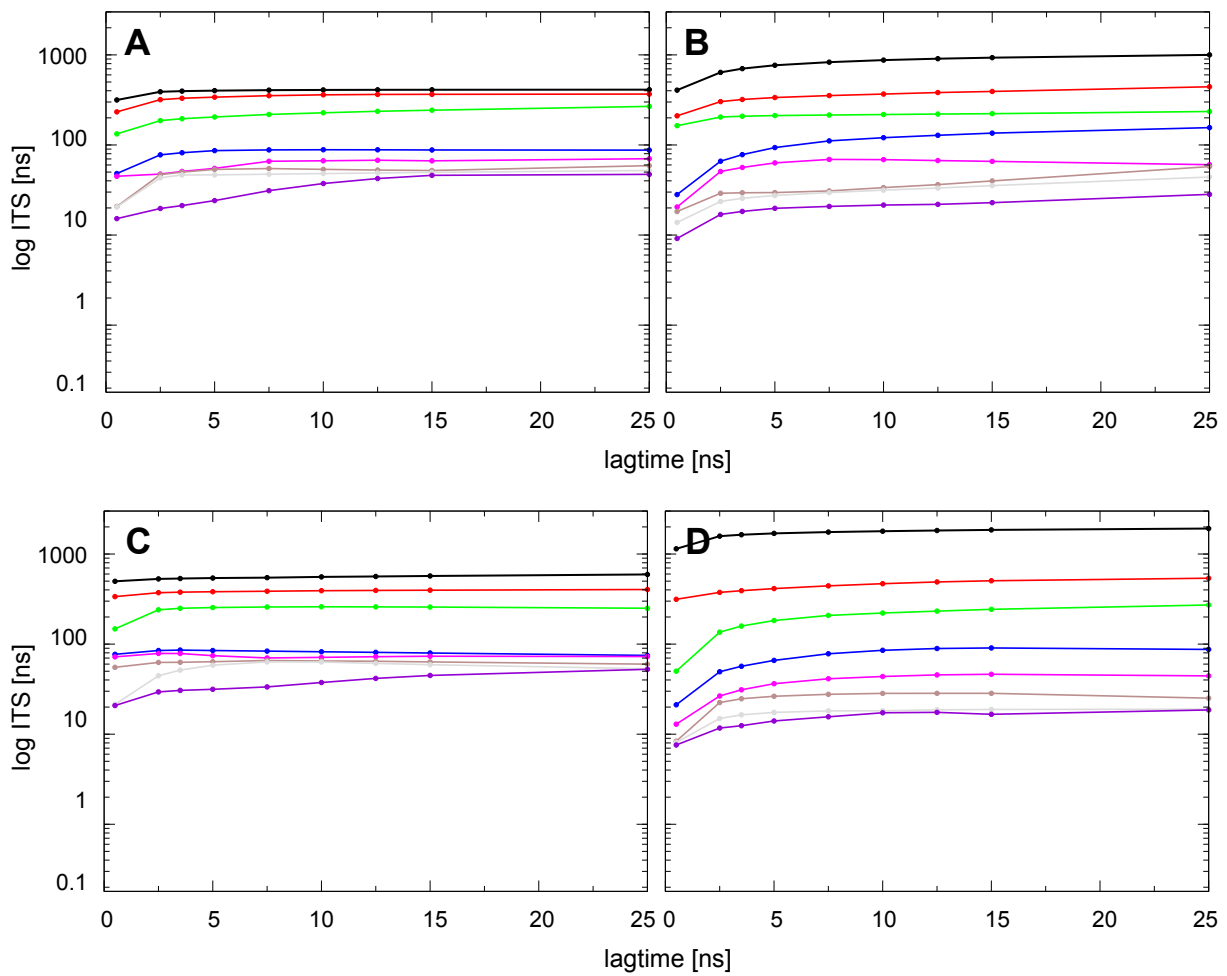


Figure S6: Implied time scales (ITS) for the interconversion processes of CsE as described by MSMs in (A) chloroform, (B) water, (C) tetrachlorocarbon (CCl₄), and (D) dimethyl sulfoxide (DMSO).

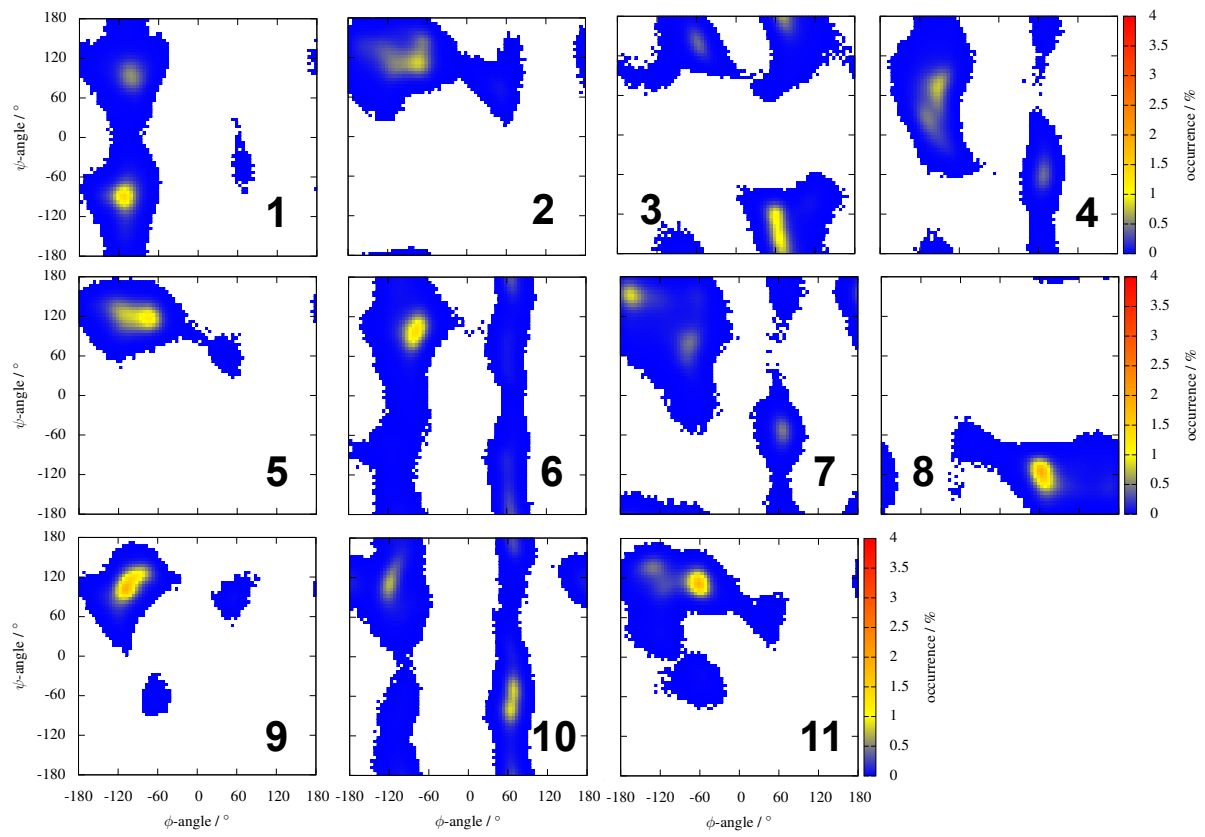


Figure S7: Ramachandran plots for the backbone torsion angles from 10 μ s simulations of CsE in chloroform.

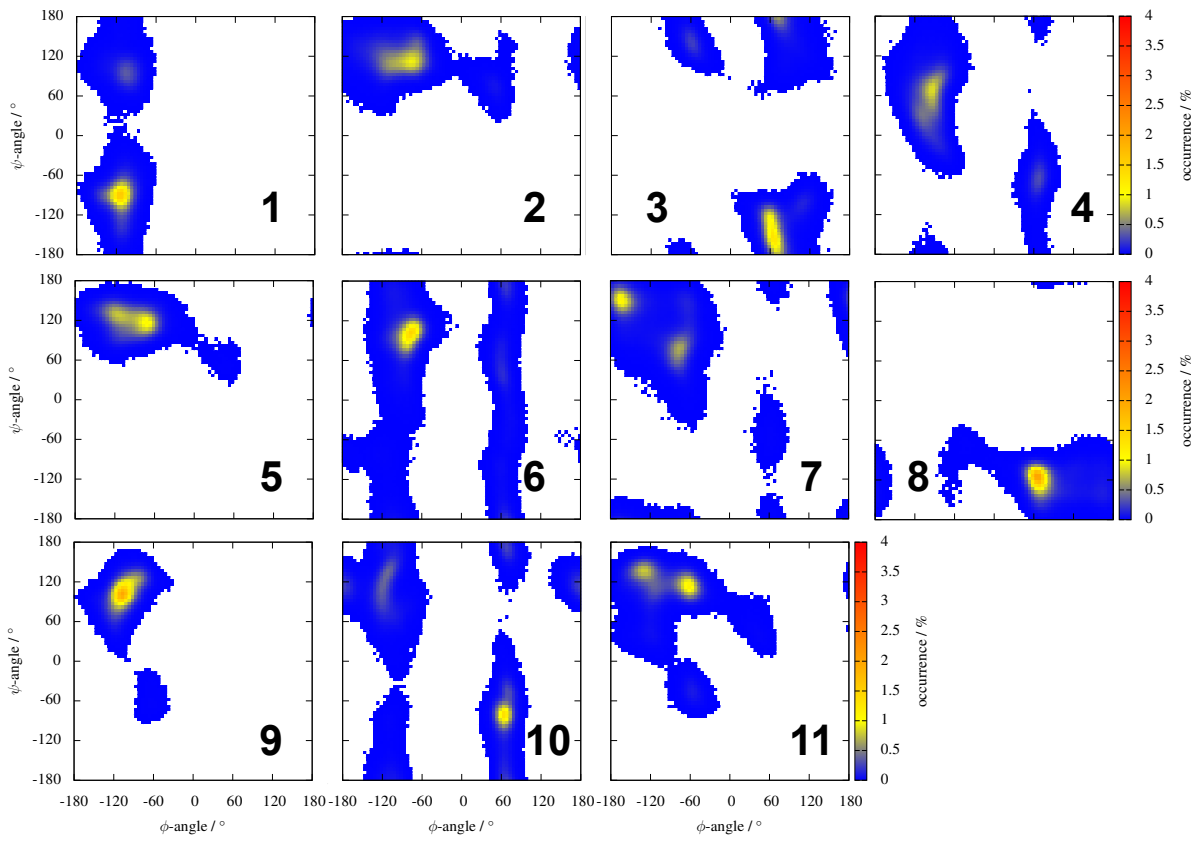


Figure S8: Ramachandran plots for the backbone torsion angles from 10 μs simulations of CsE in tetrachlorocarbon (CCl_4).

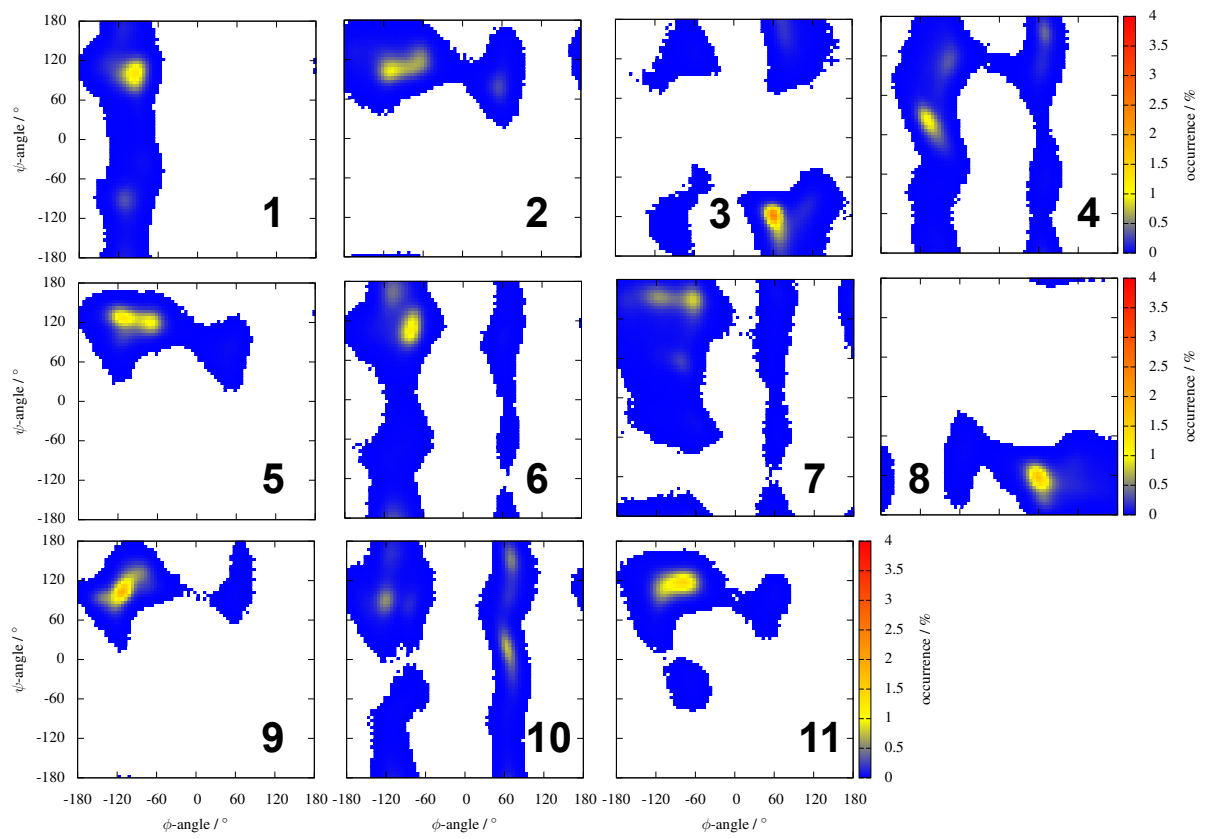


Figure S9: Ramachandran plots for the backbone torsion angles from 20 μ s simulations of CsE in water.

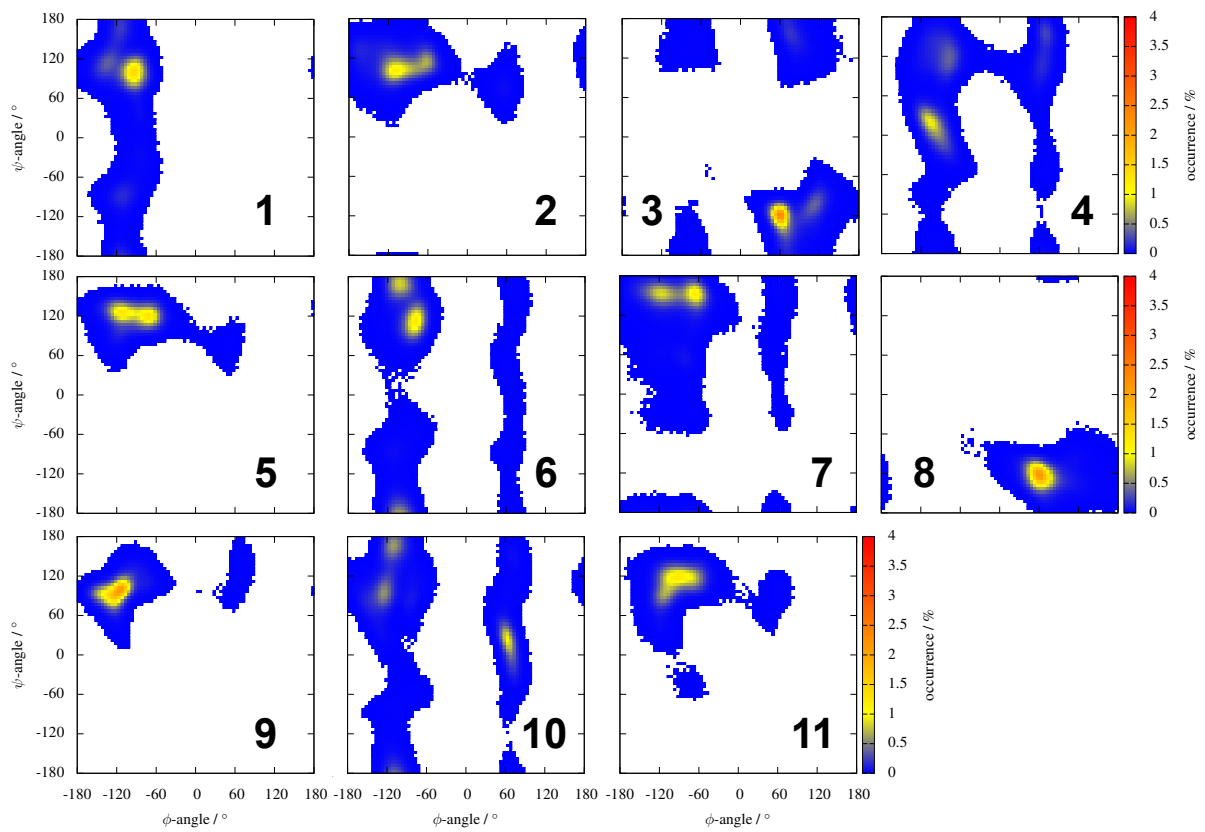


Figure S10: Ramachandran plots for the backbone torsion angles from 20 μ s simulations of CsE in dimethyl sulfoxide (DMSO).

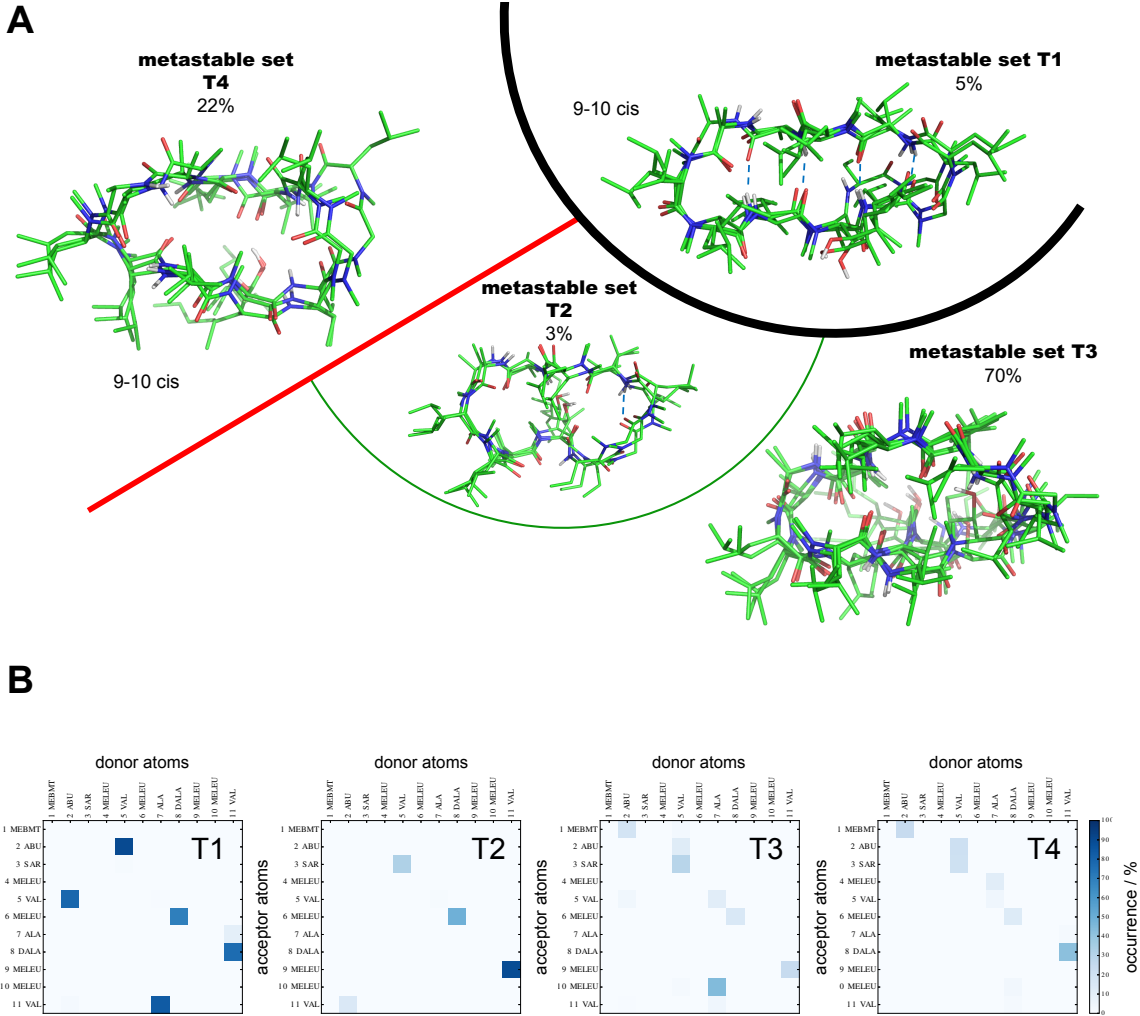


Figure S11: (A) Schematic representation of the metastable sets in tetrachlorocarbon (CCl_4): T1, T2, T3 and T4. The colors of the dividing lines correspond to the implied timescales plots in Fig. S6C. The structures shown are the centroids of clusters corresponding to the two most abundant microstates in T1, T2 and T4 and the 7 most abundant microstates in T3 (generated using PyMOL³⁶). (B) Intramolecular backbone–backbone H-bonds.

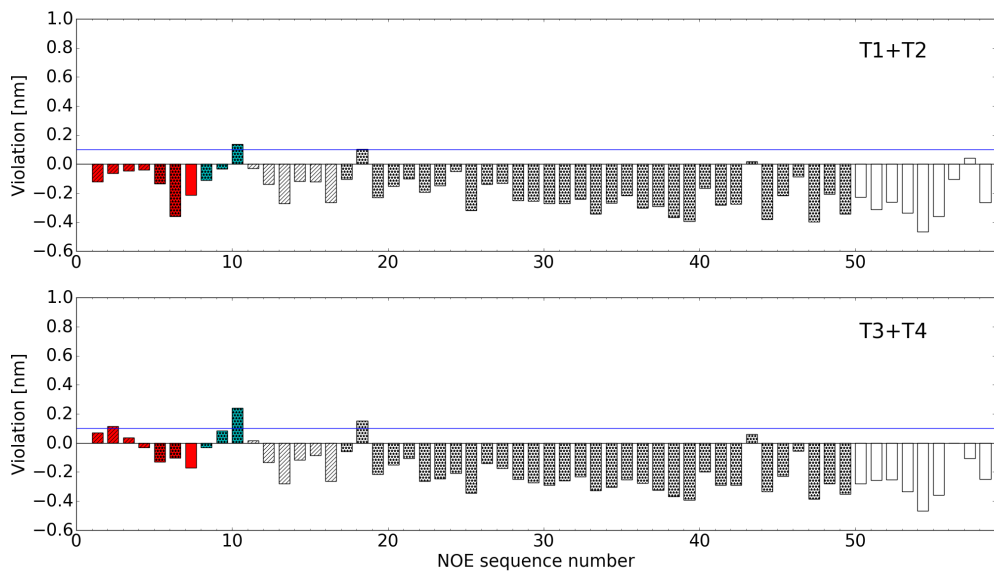


Figure S12: Violations of the experimental tetrachloromethane NOE upper distance bounds in the $10\ \mu\text{s}$ simulation of CsE in tetrachlorocarbon (CCl_4). (Top): Metastable sets T1 and T2. (Bottom): Metastable sets T3 and T4. The NOE distances are grouped into “intercycle” (red), “intermediate” (cyan) and “vicinal” (white), and they are labelled on the basis of nature of the hydrogens: backbone–backbone (stripes), backbone–side chains (dot) and side chain–side chain (plain).

References

- (1) Vonkienlin, M.; Moonen, C. T. W.; Vandertoorn, A.; Vanzijl, P. C. M. *J. Magn. Reson.* **1991**, *93*, 423–429.
- (2) Carpenter, T. A.; Colebrook, L. D.; Hall, L. D.; K.Pierens, G. *Magn Reson Chem* **1992**, *30*, 768–773.
- (3) Kay, L. E.; Keifer, P.; Saarinen, T. *J. Am. Chem. Soc.* **1992**, *114*, 10663–10665.
- (4) Kupce, E. *Method. Enzymol.* **2001**, *338*, 82–111.
- (5) Bax, A.; Summers, M. F. *J. Am. Chem. Soc.* **1986**, *108*, 2093–2094.
- (6) Meissner, A.; Sorensen, O. W. *Magn. Reson. Chem.* **2000**, *38*, 981–984.

- (7) Bax, A.; Davis, D. G. *J. Magn. Reson.* **1985**, *63*, 207–213.
- (8) Hwang, T. L.; Shaka, A. J. *J. Am. Chem. Soc.* **1992**, *114*, 3157–3159.
- (9) Bax, A.; Davis, D. G. *J. Magn. Reson.* **1985**, *65*, 355–360.
- (10) Meissner, A.; Sorensen, O. W. *Magn. Reson. Chem.* **2001**, *39*, 49–52.
- (11) Gottlieb, H. E.; Kotlyar, V.; Nudelman, A. *J. Org. Chem.* **1997**, *62*, 7512–7515.
- (12) Herrmann, T.; Güntert, P.; Wüthrich, K. *J. Biomol. NMR* **2002**, *24*, 171–189.
- (13) Herrmann, T.; Güntert, P.; Wüthrich, K. *J. Mol. Biol.* **2002**, *319*, 209–227.
- (14) Güntert, P. *Methods Mol. Biol.* **2004**, *278*, 353–378.
- (15) Pearlman, D. A.; Case, D. A.; Caldwell, J. W.; Ross, W. S.; III, T. E. C.; DeBolt, S.; Ferguson, D.; Seibel, G.; Kollman, P. *Comp. Phys. Commun.* **1995**, *91*, 1–41.
- (16) Bashford, D.; Case, D. A. *Annu. Rev. Phys. Chem.* **2000**, *51*, 129–152.
- (17) Lindorff-Larsen, K.; Piana, S.; Palmo, K.; Maragakis, P.; Klepeis, J. L.; Dror, R. O.; Shaw, D. E. *Proteins* **2010**, *78*, 1950–1958.
- (18) Wang, J.; R. M. Wolf, P. A. K., J. W. Caldwell; Case, D. A. *J. Comput. Chem.* **2004**, *25*, 1157–1174.
- (19) Darden, T.; York, D.; Pedersen, L. *J. Chem. Phys.* **1993**, *98*, 10089–10092.
- (20) Ryckaert, J.-P.; Ciccotti, G.; Berendsen, H. J. C. *J. Comput. Phys.* **1977**, *23*, 327–341.
- (21) Schmid, N.; Christ, C. D.; Christen, M.; Eichenberger, A. P.; van Gunsteren, W. F. *Comp. Phys. Comm.* **2012**, *183*, 890–903.
- (22) Schmid, N.; Eichenberger, A. P.; Choutko, A.; Riniker, S.; Winger, M.; Mark, A. E.; van Gunsteren, W. F. *Eur. Biophys. J.* **2011**, *40*, 843–856.

- (23) Husak, M.; Kratochvil, B.; Buchta, M.; Cvak, L.; Jegorov, A. *Collect. Czech. Chem. Commun.* **1998**, *63*, 115–120.
- (24) Kajitani, K.; Fujihashi, M.; Kobayashi, Y.; Shimizu, S.; Tsujimoto, Y.; Miki, K. *Proteins* **2008**, *70*, 1635–1639.
- (25) Woods, C. J.; Essex, J. W.; King, M. A. *J. Phys. Chem. B* **2003**, *107*, 13703–13710.
- (26) Hansmann, U. H. E. *Chem. Phys. Lett.* **1997**, *281*, 140–150.
- (27) RDKit: Cheminformatics and machine learning software. 2017; <http://www.rdkit.org>, Accessed 24.07.2017.
- (28) Deuflhard, P.; Weber, M. *Linear Algebra Appl.* **2005**, *398*, 161–184.
- (29) Chodera, J. D.; Singhal, N.; Pande, V. S.; Dill, K. A.; Swope, W. C. *J. Chem. Phys.* **2007**, *126*, 155101.
- (30) Keller, B.; Daura, X.; van Gunsteren, W. F. *J. Chem. Phys.* **2010**, *132*, 074110.
- (31) Schütte, C.; Fischer, A.; Huisenga, W.; Deuflhard, P. *J. Comput. Phys.* **1999**, *51*, 146–168.
- (32) Weber, M. *Improved Perron Cluster Analysis*; ZIB: Berlin, Germany, 2003.
- (33) Habeck, M.; Rieping, W.; Nilges, M. *J. Magn. Reson.* **2005**, *177*, 160–165.
- (34) Loosli, H.-R.; Kessler, H.; Oschkinat, H.; Weber, H.-P.; Petcher, T. J.; Widmer, A. *Helv. Chim. Acta* **1985**, *68*, 682–704.
- (35) Witek, J.; Keller, B. G.; Blatter, M.; Meissner, A.; Wagner, T.; Riniker, S. *J. Chem. Inf. Model.* **2016**, *56*, 1547–1562.
- (36) Schrödinger, LLC, The PyMOL Molecular Graphics System, Version 1.8. 2015.